Solvent effect on translational diffusivity and orientational mobility of polymers in solution: A molecular dynamics study

Ivet Bahar, Bertan Badur, and Pemra Doruker
Department of Chemical Engineering and Polymer Research Center, Bogazici University, and TUBITAK Advanced Polymeric Materials Research Center, Bebek 80815, Istanbul, Turkey

(Received 15 May 1992; accepted 15 April 1993)

Molecular dynamics simulations have been performed for a bead–spring model chain of 30 beads immersed in 738 solvent molecules. The solvent–solute interaction energy ε_{bs} has been varied in the range $0.1 \leqslant \varepsilon_{bs} \leqslant 0.8$ kcal/mol to assess the role and importance of solvent type on the dynamic and equilibrium properties of the chain. Radial distribution functions for polymer bead–solvent and bead–bead pairs indicate the enhancement of more expanded chain configurations with increasing quality of the solvent. The translational diffusivity D of the chain exhibits an inverse linear dependence on ε_{bs}, thus decreasing in the presence of more favorable polymer–solvent interactions. Molecular dimensions of the chain such as the mean-square end-to-end distance $\langle r^2 \rangle$ and the radius of gyration R_g are examined in various solvent environment. The ratio $\langle r^2 \rangle / R_g^2$ approximates the limiting value of 6 corresponding to infinitely long freely jointed chains. A linear dependence of D on $1/R_g$ is observed, in conformity with the Zimm theory of dilute polymer solutions subject to hydrodynamic interactions. The orientational motion of internal chain vectors is also found to slow down with increasing strength of intermolecular interactions, in parallel with the translational diffusivity. Characteristic orientational relaxation times τ are calculated for chain segments of various sizes n, using the initial decay rates of the corresponding orientational autocorrelations functions. These are found to obey a scaling law of the form $\tau \sim n^a$ for a given ε_{bs}. The exponent a therein decreases with the quality of the solvent, assuming values in the interval $1.0 \leqslant a \leqslant 1.5$ throughout the investigated range of polymer–solvent interactions.

I. INTRODUCTION

Most analytical treatments of polymer configurational statistics are based on *ideal chain* models, in which the specific solvent effect and the intramolecular volume exclusion are neglected.[1] Yet, the perturbations in chain equilibrium and dynamic properties arising from those effects are widely recognized.[2–8] Models based on single chain statistics are applicable, in a strict sense, only in particular cases such as dilute polymer–solvent systems under *theta* conditions, or polymers in the bulk state where a given chain does not distinguish between the surrounding molecules and intramolecular chain segments. Otherwise, the intrachain excluded volume effect and the specific solvent–polymer interaction need be considered as essential requirements for the realistic estimation of the static and dynamic properties of polymers in solution.

Simulation of polymer–solvent systems is a useful tool to investigate the behavior of polymers in various environment.[9,10] Among various computational methods, Monte Carlo generations do not generally supply information on chain dynamics, except for dynamic Monte Carlo studies[11] coupled with Metropolis algorithm which have proven useful for probing the dynamics of polymeric systems. Brownian simulations do reproduce most of time-dependent processes and are particularly useful for the study of relaxation phenomena with time scales on the order of nanoseconds; however, the solvent bombardments are approximated therein by a normal noise only, and an adjustable friction coefficient is adopted for representing the effective frictional drag of the surroundings. Those two limitations render this method inappropriate for the assessment of specific solvent effect. In this respect, molecular dynamics (MD) simulations, which consider precisely the interaction between the individual constituents of a mixture, are particularly suitable. This method will be presently employed. It is noted that that the intrachain excluded volume effect is also inherently present in MD simulations, as interactions between all nonbonded units along the chain are explicitly accounted for.

Molecular dynamics has proven to be a valuable tool for understanding the mechanism and evolution of several time-dependent processes in polymeric systems, such as orientational and translational motions in solution[12–18] or in the bulk state,[19,20] freezing in of internal rotational motions near the glass transition,[21] diffusion of simple gas molecules in polymer matrix,[22,23] cooperative transitions of bonds between rotameric states in isolated chain segments,[23–27] viscoelastic behavior of amorphous polymers under stress.[28] The model chains used in MD simulations are selected at different levels of sophistication depending on the specific properties under study. Bead–rod model chains (or Kuhn equivalent freely jointed chain) and bead–spring chains are classical examples which have been adopted in early simulations of chain dynamics,[12,13,29] and continue to be explored.[14–18] These simple models are particularly suitable for verifying various scaling arguments[30] and/or for establishing some concise analytical expressions relating chain size to static and dynamic characteristics. The bead–spring model will be adopted here to investigate

 0021-9606/93/99(3)/2235/12/$6.00 © 1993 American Institute of Physics

Downloaded 08 Jul 2003 to 136.142.92.33. Redistribution subject to AIP license or copyright, see http://ojps.aip.org/jcpo/jcpcr.jsp

the role of solvent–polymer interaction on the observed static and dynamic properties of the chain. Another group of MD studies[19–27,31–33] incorporates the structure and energy parameters of real chains, based on the rotational isomeric state model[1] of equilibrium statistics; their approach is essential for establishing the physical connection between theory and experiments, and for rationalizing the distinct behavior of different macromolecules.

Our approach closely approximates that of Luque, Santamaria, and Freire,[15] whose MD simulations indicate a systematic perturbation in chain properties due to specific solvent effect. This effect was studied in their work for a chain of $N_b=12$ beads in $N_s=343$ solvent molecules, by comparing the MD results obtained for three distinct values of solvent–polymer interaction energies. Chain dimensions (mean-square end-to-end distance $\langle r^2\rangle$ and radius of gyration R_g) and the associated relaxation times were found to increase smoothly with increasing quality of the solvent, contrasting the work of Oh, Lee, and Ree,[34] in which these properties did not exhibit a monotonous variation with solvent quality. A thorough analysis will be performed in the present work, by progressively varying the polymer–solvent interactions for a system composed of a chain of $N_b=30$ beads immersed in 738 solvent molecules. In the presence of more favorable polymer–solvent interactions, the enhanced tendency of the chain segments to maximize their contact with solvent molecules will lead to more expanded configurations, in agreement with the work of Luque *et al.*[15] The increased chain dimensions, in turn, will be shown to imply slower relaxation processes, *not only on a global scale, but also at the level of individual backbone bonds.*

Two dynamic properties will be of interest: (i) the translational diffusivity D of the overall chain, and (ii) the orientational mobility of chain segments of various sizes. The former is a global property which has been widely investigated in previous studies for chains of various lengths N_b, for the case of athermal solutions in general. The second property refers to internal conformational motions in polymers. The correct assessment of solvent effect on local conformational dynamics might be critically important for the interpretation of experiments such as NMR spectroscopy, fluorescence anisotropy, high frequency dielectric relaxation, etc., measuring characteristic relaxation times associated with short-range orientational motions in polymers. Yet, to our knowledge, no detailed MD analysis of the segmental relaxational processes in various environment has been performed so far.

Recently, Dünweg and Kremer drew attention to the occurrence of hydrodynamic interactions between the chain and its periodic images in standard MD simulations,[17] and proposed the replacement of the Oseen tensor by the corresponding Ewald sum for an accurate comparison of the results with the predictions of the Kirkwood theory. Later MD simulations of chains of various length ($6\leqslant N_b\leqslant 30$) in simulation boxes of various sizes, in the range $0.1\leqslant R_g/L\leqslant 0.3$, where L is the edge of a cubic box, indicate that such finite-system-size effects (or artifacts of periodic boundary conditions) are inconsequential insofar as the static and high frequency dynamic properties of the chain are concerned, but need be considered for a realistic interpretation of slower/global relaxational processes, such as the overall translational diffusivity of the chain.[18] The net consequence of those hydrodynamic interactions is the slowing down of the overall chain motion, in parallel with the effect of an increased concentration. A practical approach to eliminate the bias arising from finite-system-size effects, was shown to perform simulations at fixed R_g/L ratios, for a comparative analysis of the behavior of chains of various length N_b in solution. By this approach, the scaling law $D\sim N_b^{-\nu}$, in which the exponent takes on the Zimm value $\nu\approx 0.6$ in good solvent and 0.5 in theta solvent, has been verified for polymer solutions subject to hydrodynamic interactions.[18]

In view of these arguments, the correct origin of the reduced mobility of the chain in good solvent environment, which is observed in the present work, will be thoroughly analyzed. Inasmuch as the finite-size effect is negligibly small in the case of high frequency motions, the MD results obtained for highly localized motions need not be examined along these lines. However, the center of mass diffusion might be perturbed by this effect. Clearly, the chain expansion in good solvent leads to an increase in the radius of gyration and/or the hydrodynamic radius, even in infinitely dilute solution, and hence to a slowing down of chain motion in general. However, the enhancement of the possible hydrodynamic interactions with the image beads may be an additional factor, now of interchain origin, further reducing the rate of relaxational motion of chains in highly expanded configurations. With this object in mind, some simulations are repeated by varying L and N_s, and keeping the ratio R_g/L fixed, in order to estimate the interchain hydrodynamic contribution to the observed behavior. No significant deviations in the diffusivity could be observed—other than those within statistical errors of Green–Kubo integration results—for the chain of $N_b=30$ units, upon varying the size of the simulation box in the range $0.15\leqslant R_g/L\leqslant 0.25$. Although a weak tendency to move faster in a larger box or vise versa is discernible, the contribution of this effect to the observed behavior is minor, and we conclude that in the investigated concentration regime the decrease in chain mobility is mostly affected by local solvent polymer interaction rather than occasional interactions with image beads. Besides, it should be recognized that for a solution with fixed concentration, possible increases in hydrodynamic interactions due to configurational expansions in good solvent, and the associated decrease in chain diffusivity, *do exist* and need not necessarily be viewed as artifacts of simulations. They should certainly be considered when interpreting the results in terms of the Kirkwood formalism, inasmuch as the effective hydrodynamic radius is modified. However, the possible slowing down of the chain, arising from enhanced polymer–polymer interactions, might be viewed as an indirect consequence of the configurational expansion of the chain in response to good solvent conditions, in a system of fixed concentration.

Downloaded 08 Jul 2003 to 136.142.92.33. Redistribution subject to AIP license or copyright, see http://ojps.aip.org/jcpo/jcpcr.jsp

II. MODEL AND METHOD

A. General approach

The system consists of $N_s=738$ solvent molecules and a polymer chain of $N_b=30$ beads, each of equal mass m. A cubic simulation box composed of body-centered cubic (bcc) lattice sites is adopted for describing the original coordinates of the set of $N_b+N_s=N$ particles. The box is subject to periodic boundary conditions. The particles are originally placed at the centers and four of the corners along opposite diagonals of each bcc lattice site, thus leading to a tetrahedral arrangement for the polymer bonds in their original state. This structure will be certainly lost during simulation but such a symmetric arrangement of chain beads at start has the advantage of necessitating shorter equilibration period compared to randomly placed beads. Following this prescription, each site accommodates 1.5 particles. Thus the set of $N=768$ particles considered in the majority of simulations results from a cubic box of 8 bcc sites along each edge. The first bead of the polymer chain and the particular sequence of connected beads are selected by a random number generator subroutine. Accordingly, for the choice of the bead $i+1$ along the chain, the random number generator assigns one tetrahedral directional vector among those (three or less) accessible to bead i. The term accessible refers here to those directional vectors leading to sites which are not already occupied by the previously selected beads. The position vector of the ith particle (polymer bead or solvent) is denoted by $\mathbf{r}_i$, with respect to the laboratory-fixed frame whose origin is conveniently located at the center of the simulation box. The initial velocities are assigned in conformity with the Boltzmann distribution at the simulation temperature. The net linear momentum is set equal to zero by subtracting the mean velocity from the individual velocities at each step. Isothermal conditions are maintained by monitoring and rescaling the velocities of the particles at regular time intervals. Inasmuch as the total energy is also conserved along the trajectory, the resulting averages approximate the behavior of an isoenthalpic-canonical ensemble. Velocity rescaling to correct for thermal drift is of negligible consequence in the case of *stationary processes* and has been commonly used in previous MD studies.[35–37] However, it is noted that more rigorous approaches[38,39] become mandatory for the constant temperature and/or pressure simulation of *nonequilibrium processes* such as chemical reactions and phase changes.

B. Interaction energies

The interaction between the nonbonded pair of particles i and j at a distance $r_{ij}\equiv|\mathbf{r}_j-\mathbf{r}_i|$ from each other is taken to be of the form of the shifted-force potential[9]

$$V_{SF}(r_{ij})=\begin{cases}V_{LJ}(r_{ij})-V_{LJ}(r_c)-(r_{ij}-r_c)(dV_{LJ}(r_{ij})/dr_{ij})_{r_{ij}=r_c} & r_{ij}\leqslant r_c\\ 0 & r_{ij}>r_c\end{cases}, \tag{1}$$

where $V_{LJ}(r_{ij})$ is the Lennard-Jones (LJ) (6–12) potential given by

$$V_{LJ}(r_{ij})=4\varepsilon_{ij}[(\sigma_{ij}/r_{ij})^{12}-(\sigma_{ij}/r_{ij})^{6}] \tag{2}$$

and r_c is the cutoff distance beyond which the interaction vanishes. ε_{ij} and σ_{ij} in Eq. (2) are the respective energy and distance parameters corresponding to the particular pair of particles i and j. The adoption of a cutoff separation introduces discontinuities in the absolute value and slope of the interaction energy at r_c, which are eliminated by the addition of the last two terms in Eq. (1). Minimum image convention is used for the specification of r_{ij}.[9] The subscripts i and j of the above variables will be replaced by either s (solvent) or b (polymer bead) depending on the type of interacting particles. The van der Waals radii and consequently the length parameters of polymer beads and solvent molecules will be assumed to be equal to each other. Thus the subscript ij in the LJ length parameter σ_{ij} will be omitted for brevity. The cutoff separation is taken as $r_c=2.5\,\sigma$. The elastic potential of the ith spring is given by the so-called finitely extendable nonlinear elastic or FENE potential[40–42]

$$V_{QH}(l_i)=-0.5k_0\,l_0^2\ln[1-(l_i/l_0)^2] \quad l_i<l_0,$$
$$V_{QH}(l_i)=\infty \quad l_i\geqslant l_0, \tag{3}$$

where l_i is the instantaneous length of the ith spring. The subscript QH refers to the quasiharmonic nature of the potential. k_0 and l_0 are the energy and length parameters of the quasiharmonic potential, respectively. The above form of connector potential has found widespread use in previous MD studies of polymer solutions.[13,15,17] This function is monotone strictly increasing with l_i, thus favoring small extensions and eventual overlap of the beads. Yet, the beads can not actually approach each other by more than some limiting separation, as inherently implemented by the shifted potential function of Eq. (1), which applies to all pairs of nonbonded beads. Thus the total potential of the polymer chain results from the contributions of both Eqs. (1) and (3), summed over all relevant pairs. For a system composed of a single polymer chain surrounded by solvent molecules, the total interaction energy reads

$$U=\sum_{i=1}^{N-1}\sum_{j=i+1}^{N}V_{SF}(r_{ij})+\sum_{k=1}^{N_b-1}V_{QH}(l_k). \tag{4}$$

Downloaded 08 Jul 2003 to 136.142.92.33. Redistribution subject to AIP license or copyright, see http://ojps.aip.org/jcpo/jcpcr.jsp

TABLE I. Simulation parameters and reduced variables.[a]

Real variables and absolute values		Dimensionless variables and reduced values	
Particle mass, m	$(12/N_A)$ g	$m_r=m/m^*$	1
LJ length parameter, σ	2.7 Å	$\sigma_r=\sigma/\sigma^*$	1
QH length parameter, l_0	5.265 Å	$l_{0r}=l_0/\sigma^*$	1.95
Temperature, T	378 K	$T_r=RT/\epsilon^*$	0.75
Box volume, $V=L^3$	$(24.3$ Å$)^3$	$V_r=V/\sigma^{*3}$	9.0^3
Number density; $\rho=N/V$	0.0535 Å^{-3}	$\rho_r=\rho\sigma^{*3}$	1.054
Time step, Δt	4.57 fs	$\Delta t_r=\Delta t/(\sigma^{*2}m^*N_A/\epsilon^*)^{1/2}$	0.01
LJ energy parameter, ϵ_{bb}	0.5 kcal	$\epsilon_{bbr}=\epsilon_{bb}/\epsilon^*$	0.5
LJ energy parameter, ϵ_{ss}	0.5 kcal	$\epsilon_{ssr}=\epsilon_{ss}/\epsilon^*$	0.5
LJ energy parameter, ϵ_{bs}	0.1–0.8 kcal	$\epsilon_{bsr}=\epsilon_{bs}/\epsilon^*$	0.1–0.8
QH energy parameter, k_0	$20\epsilon_{bb}/\sigma^2$	$k_{0r}=k_0\sigma^{*2}/\epsilon^*$	10

[a]N_A=Avogadro number. Reference values: $m^*=(12/N_A)$ g; $\sigma^*=2.7$ Å; $\epsilon^*=1.0$ kcal. Other reduced variables: $\mathbf{r}_{ir}=\mathbf{r}_i/\sigma^*$; $\mathbf{v}_{ir}=\mathbf{v}_i(m^*N_A/\epsilon^*)^{1/2}$; $\mathbf{a}_{ir}=\mathbf{a}_i\sigma^*m^*N_A/\epsilon^*$.

The first summation in Eq. (4) is performed over all of the N particles present in the simulation box, except for the first neighboring beads along the chain. The second term accounts for the quasiharmonic potential of the springs.

C. Simulation algorithm and parameters

The equation of motion for the ith particle, $1\leqslant i\leqslant N$, reads

$$m_i\mathbf{a}_i=\mathbf{f}_i=-\nabla_{\mathbf{r}_i}U, \tag{5}$$

where $m_i=m$ is the mass of particle i, $\mathbf{f}_i$ is the force exerted on particle i, $\mathbf{a}_i$ is its acceleration, and $\nabla_{\mathbf{r}_i}U$ is the gradient of the potential U with respect to $\mathbf{r}_i$. The modified Verlet approach with the recurrence equations given by[9,43]

$$\begin{aligned}\mathbf{r}_i(t+\Delta t)&=\mathbf{r}_i(t)+\Delta t\mathbf{v}_i(t)+\tfrac{2}{3}(\Delta t)^2\mathbf{a}_i(t)\\&\quad-\tfrac{1}{6}(\Delta t)^2\mathbf{a}_i(t-\Delta t),\\\mathbf{v}_{ir}(t+\Delta t)&=\mathbf{v}_i(t)+\tfrac{1}{3}\Delta t\mathbf{a}_i(t+\Delta t)+\tfrac{5}{6}\Delta t\mathbf{a}_i(t)\\&\quad-\tfrac{1}{6}\Delta t\mathbf{a}_i(t-\Delta t)\end{aligned} \tag{6}$$

has been used. Here $\mathbf{v}_i(t)$ is the velocity of particle i at time t, and Δt is the size of the time step. This algorithm, in which the acceleration $\mathbf{a}_i(t-\Delta t)$ is stored in addition to $\mathbf{r}_i(t)$, $\mathbf{v}_i(t)$, and $\mathbf{a}_i(t)$, allows for a more accurate estimation of velocities compared to the classical Verlet method, and consequently brings about an improvement in energy conservation.[9]

The recurrence equations given by Eq. (6) may be identically rewritten in terms of reduced variables listed in Table I. The parameters m^*, σ^*, and ε^* therein represent the reference values which are used to obtain the reduced variables. The values of the parameters used in simulations are listed in Table I, as well as the expressions and values for their reduced counterparts, indicated with the subscript r. The expression for the reduced velocity $\mathbf{v}_{ir}$ follows from the broadening of the Gaussian distribution of velocities by a factor of $(m^*N_A/\varepsilon^*)^{1/2}$ due to the use of reduced temperature and mass in the Maxwell–Boltzmann expression. The LJ parameter ε_{bs} is subjected to variations within the range $0.1\leqslant\varepsilon_{bs}\leqslant0.8$ kcal/mol, while the other two interaction potentials are kept fixed at $\varepsilon_{bb}=\varepsilon_{ss}=0.5$ kcal/mol. The reduced number density $\rho_r=1.054$ is equivalent to an absolute mass density ρ_m of 1.07 g/cm^3, as follows from the identity $\rho_m=NmN_A/L^3$. The values $L=9\sigma^*$ and $N_s=738$ have been used in the simulations, except for a few runs performed with the aim of estimating the role of hydrodynamic interactions, as will be indicated. Table II illustrates for three selected values of ε_{bs}, namely, 0.2, 0.5, and 0.8 kcal/mol, the mean values and standard deviations of different types of energies, resulting from short runs of 10^4 steps. The quasiharmonic potential energies V_{QH} listed in the second column represent the average over the trajectory and over the N_b-1 springs. The temperatures were rescaled every 200 time steps. The shifted force potentials V_{SF} and the kinetic energies correspond to averages over all units, i.e. polymer beads and solvents. The negative values for the mean V_{SF} indicates that, in general, favorable interactions, i.e. good solvent conditions, are brought about by the present choice of simulation parameters.

III. RESULTS AND DISCUSSION

In general, an increase in ε_{ij} strengthens the interaction, both attractive and repulsive, between particles i and j. However, the attractive portion of the LJ energy curves is more sensitive to ε_{ij} while the steep change in the repulsive regime is weakly affected. Thus the effective change brought about by an increase in ε_{ij} is to enhance the favorable interaction between particle i and j, as may be verified from the V_{SF} values listed in Table II. Accordingly, a lower value for ε_{bs} should give rise to a more compact

TABLE II. Mean energies (kcal) per unit[a] and their standard deviations.

ϵ_{bsr}		V_{QH}	V_{SF}	Kinetic	T_r
0.2	MEAN	2.072	−0.096	1.125	0.750
	S.D.	0.051	0.009	0.026	0.017
0.5	MEAN	2.070	−0.197	1.125	0.750
	S.D.	0.057	0.008	0.026	0.017
0.8	MEAN	2.023	−0.343	1.125	0.750
	S.D.	0.062	0.010	0.027	0.018

[a]Units refer to polymer springs in the case of quasiharmonic (QH) potentials; both solvent molecules and polymer beads for shifted force potentials and kinetic energies, on molar basis.

Downloaded 08 Jul 2003 to 136.142.92.33. Redistribution subject to AIP license or copyright, see http://ojps.aip.org/jcpo/jcpcr.jsp

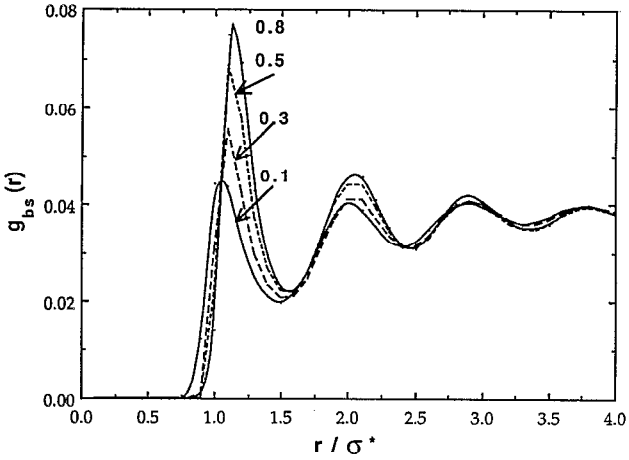

FIG. 1. Radial distribution function $g_{bs}(r)$ from MD simulations for solvent molecule–polymer bead pair as a function of the reduced separation r/σ^*. Results are shown for systems subject to distinct reduced polymer–solvent interaction parameters $\varepsilon_{bs}{}^*\equiv\varepsilon_{bs}/\varepsilon^* = 0.1$, 0.3, 0.5, and 0.8, as indicated, using the simulation data given in Table I. Intermolecular separations are observed to increase with decreasing quality of the solvent, i.e., with increasing ε_{bs} values.

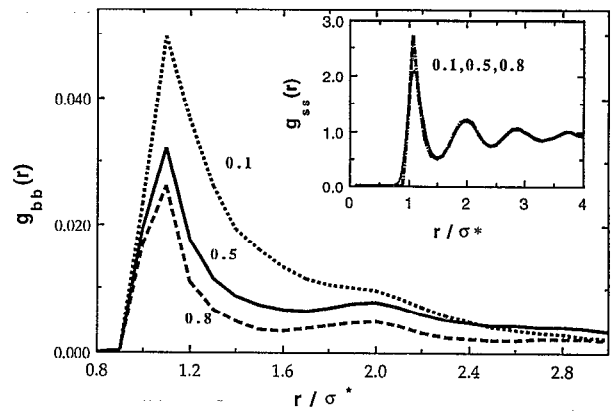

FIG. 2. Radial distribution function $g_{bb}(r)$ from MD simulations for pairs of non bonded beads of polymer chain as a function of the reduced separation r/σ^*. Results are shown for the reduced polymer–solvent interaction parameters $\varepsilon_{bs}/\varepsilon^*=0.1$, 0.5, and 0.8. The upper small diagram on the right is obtained with the same set of data and illustrates the insensitivity of solvent–solvent pair correlation function $g_{ss}(r)$ to polymer–solvent interaction.

chain configuration. With these qualitative features in mind, we now turn our attention to the influence of solvent–polymer interaction on various properties.

1. Radial distribution functions

The radial distribution function $g_{ij}(r)$, also referred to as pair-correlation function, gives the unnormalized probability of finding a pair of particles i and j a distance r apart. $g_{ij}(r)$ is evaluated from

$$g_{ij}(r)=(\rho^{-1}/N)\langle n_{ij}(r)\rangle/(4\pi r^2\Delta r), \tag{7}$$

where the number $\langle n_{ij}(r)\rangle$ of particles located at a distance r from each other is found from the time average of $n_{ij}(r)=2\int d\mathbf{r}\Sigma_i\Sigma_{j\neq i}\delta(\mathbf{r}-\mathbf{r}_i+\mathbf{r}_j)$. This integration is performed over a thin spherical shell of thickness Δr, about $\mathbf{r}$, and the summations of the delta functions include all pair of particles of type i and j with $j\neq i$, changing in the range $[1, N_b]$ for polymer beads and $[1, N_s]$ for solvent molecules. In the limit as r becomes infinitely large, using image particles convention throughout space, $g_{ij}(r)$ approaches the ratio N_iN_j/N^2, for $i\neq j$ and $N_i(N_i-1)/N^2$ for pairs of the same type. Thus the radial distribution curves should approach unity provided that they are normalized with respect to these asymptotic values. Both time and ensemble averages are used in evaluating $g_{ij}(r)$, leading to curves with minimal noise.

The computation of pair correlation functions from MD simulations is not new but has been performed here for an assessment of the compliance of our results with previous work,[15] and for a clear visualization of the change in intrachain separations as a function of solvent type. Figures 1 and 2 illustrate the dependences of $g_{bs}(r)$, $g_{bb}(r)$, and $g_{ss}(r)$ on solvent quality. The grid size is taken as $\Delta r=0.01\sigma^*$. Short durations of simulation ($\sim 10^4$ time steps) are found to be sufficient to reproduce—indistinguishably—each of the curves displayed in the figures. The tendency of the chain to assume more expanded configurations in good solvent, i.e., with increasing ε_{bs}, is manifested in Fig. 1 by the larger $g_{bs}(r)$ values attained at short separations in media with higher ε_{bs}, in agreement with the MD results obtained by Freire and collaborators[15] for a smaller system. We note that the successive peaks in the distribution function occur at locations $r/\sigma^*\sim 1.1$, 2.0 and 3.0, in perfect agreement with previous work, in which the same model and comparable energy and length parameters have been adopted.[15] The gradual shifting of the first peak to larger r/σ^* values with increasing ε_{bs} is also in quantitative conformity with previous MD results.[15] The oscillations of $g_{bs}(r)$ corresponding to successive shells of neighbors are observed to be stronger with increasing ε_{bs}. Weaker ε_{bs} values, on the other hand, induce less pronounced peaks associated with more randomized relative positions of particles. This feature is indicative of the increased diffusional mobility of the particles in the presence of weak intermolecular associations, which will be further exploited below.

The intrachain radial distribution function $g_{bb}(r)$ shown in Fig. 2 has been evaluated on the basis of nonbonded units along the chain. First neighboring units are not included in this analysis inasmuch as their separation is predominantly determined by the quasiharmonic potential and attention here is primarily focused on the influence of solvent quality on the spatial arrangement of the atoms/beads. The distribution of bond lengths l in response to the changes in solvent quality will be separately considered next. A strong dependence on ε_{bs} is observable in Fig. 2, in conformity with the behavior described above: The beads come closer to each other as the solvent becomes poorer. The diagram on the upper right part of Fig. 2 shows the solvent–solvent radial distribution functions $g_{ss}(r)$ which have been obtained in MD simulations, for various ε_{bs}. The

Downloaded 08 Jul 2003 to 136.142.92.33. Redistribution subject to AIP license or copyright, see http://ojps.aip.org/jcpo/jcpcr.jsp

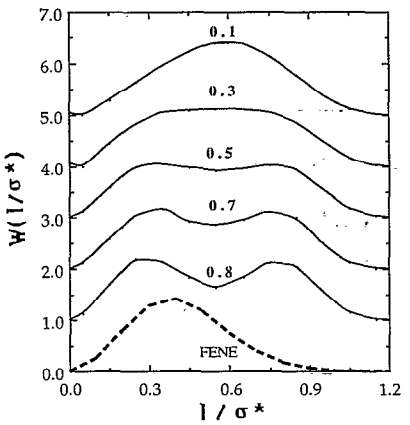

FIG. 3. Distribution $W(l)$ of bond/spring lengths l in chains subject to interactions of various strength with the surroundings. $\varepsilon_{bs}/\varepsilon^*$ values are 0.1, 0.3, 0.5, 0.7, and 0.8 as indicated by the labels on each curve. The unimodal distribution of bond lengths for low ε_{bs}, values is gradually split into two peaks as the association between solvent and polymer is strengthened. The lower dashed curve is the distribution for isolated dumbbells subject to FENE potential with the same parameters.

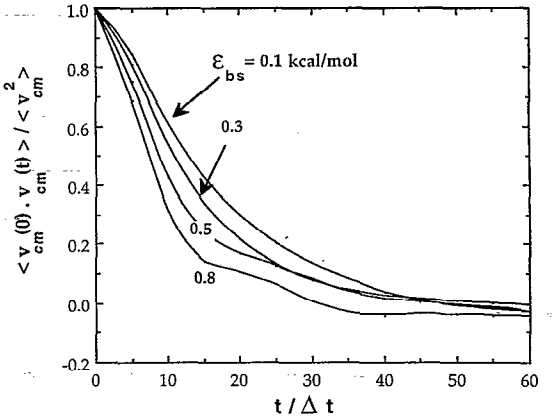

FIG. 4. Time decay of the autocorrelation function $\langle \mathbf{v}_{c.m.}(0)\cdot\mathbf{v}_{c.m.}(t)\rangle/\langle \mathbf{v}_{c.m.}^2\rangle$ of the polymer mass center velocity $\mathbf{v}_{c.m.}$. The abscissa represents the reduced time $t/\Delta t$ or the number of MD time steps. Curves are given for $\varepsilon_{bs}/\varepsilon^*=0.1$, 0.3, 0.5, and 0.8.

insensitivity of $g_{ss}(r)$ to ε_{bs} is legitimate for the highly dilute system presently investigated.

2. Equilibrium distribution of bond/spring lengths

Figure 3 displays the probability distribution $W(l/\sigma^*)$ of the reduced length l/σ^* of bonds for various ε_{bs} values. The zero level of the distribution curves are vertically shifted by a value of 1.0 for clarity. Interestingly enough, with increasing ε_{bs} the approximately Gaussian shape of the distribution is distorted into a bimodal structure. For isolated dumbbells subject to the FENE potential, the connector length distribution is given by[40]

$$W_{QH}(l_i)=J[1-(l_i/l_0)^2]^{k_0 l_0^2/2kT} \quad l_i<l_0,$$
$$W_{QH}(l_i)=0 \quad l_i\geqslant l_0, \tag{8}$$

where J is the normalization constant. The lowest dashed curve in Fig. 3 is calculated by inserting the FENE parameters of Table I, adopted in simulations, into Eq. (8) multiplied by $4\pi l_i^2$. All of the curves are normalized. Comparison of the dashed curve with those resulting from MD simulations indicates that the chain connectivity and the interaction with the surroundings substantially modify the distribution corresponding to isolated dumbbells. In general, the mean of the distribution function is shifted to larger values (i.e., from $\sim$0.40 to 0.56) when the dumbbell belongs to a chain. This shift is presumably forced by the intrachain Lennard-Jones type potential, which requires second neighboring bonds to be separated by a distance of about $2^{1/6}\sigma^*$. This requirement leads to an average separation of $0.56\sigma^*$ between adjacent beads, in exact conformity with the MD results. At $\varepsilon_{bs}=0.1\varepsilon^*$ the attractive potential of the environment is relatively weak to perturb the shape of the distribution function and a unimodal distribution centered about $0.56\sigma^*$ is observed. However, as the interaction between polymer and solvent is strengthened, the distribution is gradually modified into a bimodal shape. The peak to the right may be attributed to an increased separation between adjacent beads due to their simultaneous interaction with a single solvent molecule. These two beads that are strongly attracted to a single molecule are being forced apart by that interaction. However, when the corresponding bond assumes this increased length, its first neighbor has to assume a relatively contracted configuration in order to comply with the requirements of intrachain LJ potential between second neighbors, and hence the appearance of the accompanying peak at the left.

3. Translational diffusivity as a function of solvent–polymer interaction

The diffusion coefficient is computed from the time decay of the chain center-of-mass velocity autocorrelation function $\langle \mathbf{v}_{c.m.}(t_0)\cdot\mathbf{v}_{c.m.}(t_0+t)\rangle$ according to the Green–Kubo relationship

$$D=\frac{1}{3}\int_0^\infty \langle \mathbf{v}_{c.m.}(t_0)\cdot\mathbf{v}_{c.m.}(t_0+t)\rangle dt, \tag{9}$$

where the angular brackets refer to the time average over initial times t_0. This average relies on the independence of the dynamics of stationary processes upon the time origin. The velocity $\mathbf{v}_{c.m.}(t)$ of the polymer mass center at a given time t is found from the average of the instantaneous velocities of the N_b beads as $\mathbf{v}_{c.m.}(t)=N_b^{-1}\Sigma_i \mathbf{v}_i(t)$.

Figure 4 displays the time decay of the normalized velocity autocorrelation function of the polymer mass center, for various ε_{bs} values as indicated by the labels. The abscissa is the ratio $t/\Delta t$ of the elapsed time t to the time step Δt of simulation. Full relaxation of $\mathbf{v}_{c.m.}(t)$ is observed to occur in the range of picoseconds. The weak statistical noise of the decay curves in the long time range is minimized by taking averages over simulations with durations of about 10^5 time steps, for each ε_{bs}. The fluctuations occurring in the long time portions of the curves do not arise from any statistical uncertainties but are identically repro-

Downloaded 08 Jul 2003 to 136.142.92.33. Redistribution subject to AIP license or copyright, see http://ojps.aip.org/jcpo/jcpcr.jsp

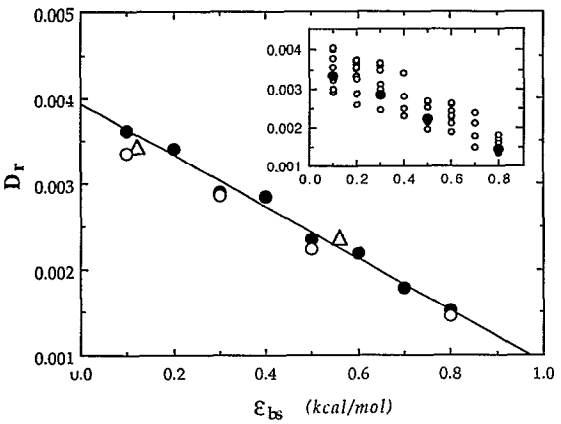

FIG. 5. Dependence of polymer translational diffusivity on solvent–polymer interaction. Reduced diffusion coefficient D_r is plotted against the polymer–solvent interaction parameter ε_{bs} (which coincides with the reduced quantity $\varepsilon_{bs}/\varepsilon^*$ as $\varepsilon^*=1$ kcal/mol). The filled circles represent the averages of several runs of 10^4 time steps performed with the data of Table I for each ε_{bs} value, which are illustrated in the upper small diagram. Best-fitting line is drawn through the MD results to guide the eye. The empty triangles represent the results obtained by keeping R_g/L fixed at $R_g/L=0.21$, and rescaling the size of the simulation box accordingly. The empty circles at $\varepsilon_{bs}/\varepsilon^*=0.1$, 0.3, 0.5, and 0.8 in the figure (and the filled circles in the upper small diagram) represent results obtained from Einstein plots illustrated in Fig. 6.

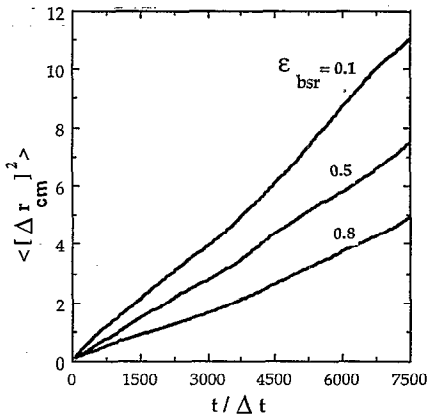

FIG. 6. Mean-square displacement of the mass center $\langle[\Delta \mathbf{r}_{c.m.}(t)]^2\rangle$ as a function of time, for polymer–solvent interaction energies $\varepsilon_{bs}=0.1$, 0.5 and 0.8 kcal/mol.

duced in repetitive runs, indicating the particular structure of the time decay of $\langle \mathbf{v}_{c.m.}(t_0)\cdot\mathbf{v}_{c.m.}(t_0+t)\rangle$. Performing a set of short runs with different original configurations rather than a single run of long duration has proven to be a computationally efficient method of determining the decay curves. The resulting translational diffusion coefficients are shown by the filled circles in Fig. 5 as a function of ε_{bs}. Results are displayed in reduced units $D_r=D(m^*N_A/\varepsilon^*)^{1/2}/\sigma^*$. Best fitting straight line is drawn through the results, to guide the eye. For illustrative purposes, the diffusion coefficients calculated from short runs of 10^4 time steps are plotted in the upper small diagram in the figure. This diagram gives an estimate of the scatter of D_r values resulting from successive runs of different original configurations. However, by taking the averages for each given ε_{bs}, the smooth linear decrease of D_r with increasing solvent quality emerges. The tendency of D_r to decrease with increasing ε_{bs} is also pointed out by Luque *et al.*[15] for shorter chains ($N_b=12$) while a similar study performed by Oh *et al.*[34] does not confirm this monotonous change. The present study indicates that numerical uncertainties are eliminated only if sufficiently long simulations with a variety of different original configurations are performed.

As a further check, the diffusion coefficients were also computed from the long time slope of the mean-square displacement of the mass center as a function of time, using the Einstein relationship

$$6\,Dt=\langle[\mathbf{r}_{c.m.}(t_0+t)-\mathbf{r}_{c.m.}(t_0)]^2\rangle=\langle[\Delta\mathbf{r}_{c.m.}(t)]^2\rangle \tag{10}$$

where $\mathbf{r}_{c.m.}$ is the instantaneous position vector of the center of mass, and the brackets refer to average over various initial times t_0. Figure 6 displays the change in $\langle[\Delta\mathbf{r}_{c.m.}(t)]^2\rangle$ as a function of time for $\varepsilon_{bs}=0.1$, 0.5 and 0.8 kcal/mol. The resulting diffusion coefficients, calculated from the slopes according to Eq. (10), are displayed by the empty circles in Fig. 5, and by the filled circles in the upper small diagram of the same figure.

4. Translational diffusivity in relation to chain dimensions

The change in the diffusivity of the polymer with the solvent quality is an effect which should be rather attributed to the change in the equilibrium spatial distribution of chain atoms in response to their interaction with the surroundings. In fact, Fig. 2 already confirmed that the interatomic separations are significantly perturbed by specific polymer–solvent interactions. These perturbations are directly reflected on chain dimensions such as the mean-square end-to-end separation $\langle r^2\rangle$ and the radius of gyration $R_g\equiv\langle s^2\rangle^{1/2}$, as presented in Table III, which in turn affects the chain diffusivity. Figure 7 displays the change in diffusivity with radius of gyration, resulting from runs performed for various ε_{bs}. The reduced diffusion coefficient is plotted therein against the reciprocal of the reduced mean-square radius of gyration, $1/\langle s^2\rangle_r^{1/2}$. $\langle s^2\rangle_r$ is computed from

$$\langle s^2\rangle_r=N_b^{-1}\sum_{i=1}^{N_b}\langle(|\mathbf{r}_i-\mathbf{r}_{c.m.}|)^2\rangle/\sigma^{*2}, \tag{11}$$

TABLE III. Mean-square chain dimensions and expansion coefficients α as a function of solvent quality.

ϵ_{bsr}	$\langle r^2\rangle$, Å^2	$\langle s^2\rangle$, Å^2	$\alpha^{2\,a}$
0.1	83.86±5.81	19.57±0.93	1.265
0.3	155.30±19.19	29.96±1.29	2.342
0.5	226.73±12.90	40.34±1.69	3.420
0.8	333.90±11.55	55.91±0.04	5.036

[a]The expansion coefficient is calculated from $\alpha^2=\langle r^2\rangle/(N_b-1)l^2$, where l is the average bond length taken as 0.56 σ^*.

Downloaded 08 Jul 2003 to 136.142.92.33. Redistribution subject to AIP license or copyright, see http://ojps.aip.org/jcpo/jcpcr.jsp

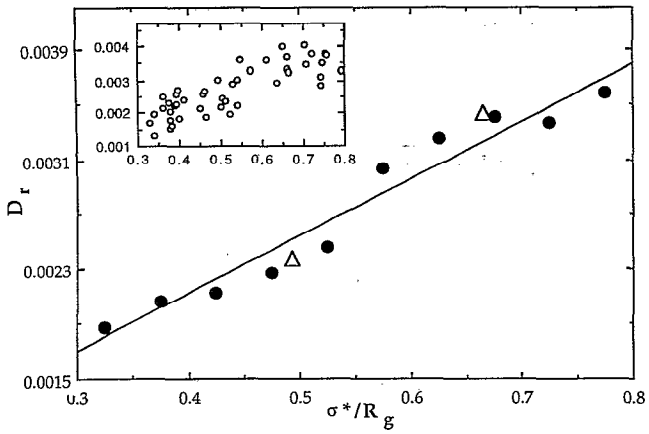

FIG. 7. Dependence of D_r on the radius of gyration R_g (or $\langle s^2\rangle^{1/2}$), irrespective of the specific solvent–polymer interaction. The abscissa is the reciprocal of the reduced radius of gyration, written as $1/\langle s^2\rangle_r^{1/2}$. Filled circles represents the averages over grids of $1/\langle s^2\rangle_r^{1/2}=0.05$ evaluated from runs of 10^5 steps, performed for various ε_{bs} values in the range $0.1\leqslant\varepsilon_{bs}\leqslant 0.8$ kcal/mol. The small diagram on the right illustrates the results from independent runs of 10^4 steps. The empty triangles are found by keeping the ratio R_g/L fixed at 0.21.

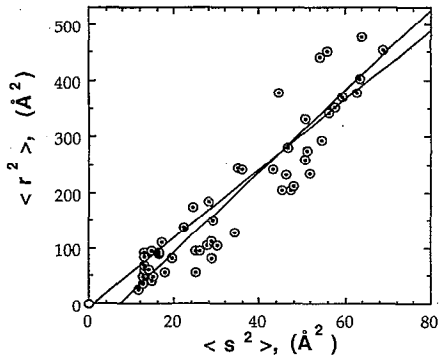

FIG. 8. Dependence of the mean-square end-to-end separation $\langle r^2\rangle$ on the radius of gyration $\langle s^2\rangle$. Circles represent time averages from independent runs of 10^4 steps evaluated irrespective of solvent–polymer interaction. The best fitting line through the data points yields a slope equal to 7.2. The second line represents the best fit for the line constrained to cross the origin and leads to $\langle r^2\rangle/\langle s^2\rangle=5.8$, in agreement with the freely jointed chain model.

where the brackets refer to time average over several snapshots in a given run. The small diagram on the right illustrates the results and their fluctuations obtained from successive runs of 10^4 steps, in parallel with Fig. 5. The filled circles in Fig. 7 represent their average values organized on the basis of grids of size $\Delta\langle s^2\rangle_r^{-1/2}=0.05$. In spite of the large scatter observed in short runs, a smooth linear dependence of D_r on $1/R_g$ follows upon consideration of simulation durations $\geqslant 10^5$ steps, as shown in the figure. The best fitting line is drawn. It is noted that here the variations in radius of gyration do not arise from any change in chain length, but from the change in the environment for a fixed chain length. Yet, the translational diffusion coefficient exhibits a linear dependence on the radius of gyration in conformity with the implications of Zimm's theory[44,45] of chain dynamics.

The ratio $\langle r^2\rangle/\langle s^2\rangle$ of the mean-square dimensions of the chains of 30 beads is found to be 6.5 ± 0.7 in the present MD simulations. This follows from the slope of the two lines drawn in Fig. 8, in which the results from several runs with various ε_{bs} are plotted. The least square fit to the data yields the line with slope 7.2. If the line is constrained to pass through the origin, on the other hand, the best fit leads to a value of 5.8. This result is in agreement with the expression $\langle r^2\rangle/\langle s^2\rangle=6N_b/(N_b+1)$ for freely jointed chains of N_b units. The slightly larger value presently obtained may be attributed to the the finite persistence length of the present relatively short chains and the excluded volume effect, which is not included in the freely jointed chain model but is implicitly present in the simulation method. It is noted that a wide range of MD values is reported in literature for the ratio $\langle r^2\rangle/\langle s^2\rangle$ of short bead–spring model chains. These deviations may be understood in view of the large amplitude scatter observed here in independent MD runs of short duration. As a final remark, we note that the systems presently studied represent good solvent conditions, as demonstrated by the expansion coefficients $\alpha>1$, listed in Table III.

It has been recently pointed out[17] that in standard MD simulations of finite-size systems subject to periodic boundary conditions, inasmuch as the infinite dilution hypothesis does not strictly hold, an *effective* hydrodynamic radius R_h, incorporating the interaction between the chain and all its images, need be computed for a correct comparison of the results with the Kirkwood theory. A practical approach to circumvent such periodic boundary artifacts in finite-size systems is asserted to perform the MD simulations at constant R_g/L ratios, when comparing the diffusivity of chains of various length.[17] This approach has recently proven useful for verifying the scaling law $D\sim N_b^{-\nu}$ or $D\sim R_g^{-1}$.[18] In view of these arguments, the influence of the finite-system-size effect on the presently obtained MD results might be questioned. In the present case, although the chain length is kept fixed, the radius of gyration changes depending on solvent quality. All simulations being carried out in the same simulation box of size $L_r^3\equiv(L/\sigma^*)^3=9.0^3$ accommodating an ensemble of 738 solvent molecules, an implicit increase in the ratio R_g/L is implemented with increasing ε_{bs}. Here the ratio R_g/L is found to increase from 0.13 to 0.29, as ε_{bs} varies from 0.1 to 0.8 kcal/mol. This increase may be partly responsible for the observed decrease of D with increasing ε_{bs}. Likewise, the observed linear dependence of D on R_g^{-1} in Fig. 7 might be biased with the same size effect, although these results are in satisfactory agreement with the predictions of the Zimm theory. As an inspection of this effect, simulations have been repeated with different box sizes, keeping on the other hand the density of the system fixed at $\rho_r=1.054$. As an illustrative example, let us consider the reference value of $R_g/L=0.21$ corresponding to the case $\varepsilon_{bs}=0.4$ kcal/mol $=0.4\varepsilon^*$. Now, if one is interested in performing the simulations at fixed R_g/L and ρ_r, this implies a *choice* of $L=6.7$ and $N_s=\rho_r L_r^3-N_b=294$ for the case $\varepsilon_{bs}=0.12\varepsilon^*$,

Downloaded 08 Jul 2003 to 136.142.92.33. Redistribution subject to AIP license or copyright, see http://ojps.aip.org/jcpo/jcpcr.jsp

for example.[46] Performing the simulations for $\varepsilon_{bs}=0.12\varepsilon^*$ with those parameters, yields the result displayed by the empty triangles at $D_r=3.34\times10^{-3}$ in Figs. 5 and 7. A weak decrease in D_r almost ranging within statistical error limits of Green–Kubo integration method, is observable. The close agreement with the original results, which were obtained with different R_g/L ratios, indicates that the size effect is practically inconsequential in the investigated R_g/L range and chain length. A further check will be to perform the simulations for the opposite case, say $\varepsilon_{bs}=0.56\varepsilon^*$ adopting now a cubic box of edge $L_r=11.2$, and $N_s=1470$, and control whether the polymer in a larger simulation box enjoys higher mobility. The result is shown by the empty triangles located at $D_r=2.28\times10^{-3}$ in Figs. 5 and 7. Only a slight tendency for increased mobility in larger box is discernible in this latter simulation, which again supports the idea that the size effect is of secondary importance in the present simulation data. It could be desirable to check the extreme case of $\varepsilon_{bs}=0.8\varepsilon^*$, as well. However, this task is not undertaken in view of (i) the high computational cost and/or less precise data collected within reasonable CPU time in this case, and (ii) the fact that the results obtained for $\varepsilon_{bs}=0.12$ and 0.56 kcal/mol do not invoke a further search in that direction.

5. Orientational autocorrelations of chain segments

For a given vector $\mathbf{m}$ in motion, the normalized orientational autocorrelation function $C(t)$ is defined as

$$C(t)=[M(t)-M(\infty)]/[M(0)-M(\infty)], \qquad (12)$$

where $M(t)\equiv\langle\mathbf{m}(0)\cdot\mathbf{m}(t)\rangle$ refers to the ensemble average over all configurational transitions. $C(t)$ reduces to $M(t)$, provided that $\mathbf{m}$ has unit magnitude. This follows from the identities $M(0)=1$ and $M(\infty)=0$, for the orientational motion of the unit vector. The time average $C(t)=\langle\mathbf{m}(t_0)\cdot\mathbf{m}(t_0+t)\rangle$ has been evaluated here on the basis of an ensemble of snapshots at various starting times t_0 as already mentioned for the mass center velocity correlation function.

The influence of solvent–polymer interaction on local motion of the chain may be surveyed from the comparative analysis of the orientational autocorrelation functions obtained for bond vectors under various ε_{bs}. Figure 9 displays the time decay of the bond autocorrelations obtained from MD runs of duration $T=2\times10^5\ \Delta t$, for each of the cases $\varepsilon_{bs}=0.2$, 0.4, and 0.6, using the simulation parameters of Table I. A significant change in local orientational mobility is observed, the motion becoming slower in the environment with larger ε_{bs}, as is conceivable in a system subject to stronger polymer–solvent attractive interactions. Figure 10 displays the time decays for a series of unit vectors $\mathbf{m}$ along the end-to-end separation of segments of n bonds, for $1\leqslant n\leqslant12$. ε_{bs} is taken as 0.2 kcal/mol, and the parameters listed in Table I are used. The autocorrelation functions displayed in Fig. 10 represent the averages over all internal chain segments, excluding the terminal four atoms at both ends of the chain, in order to eliminate the bias arising from end effects.

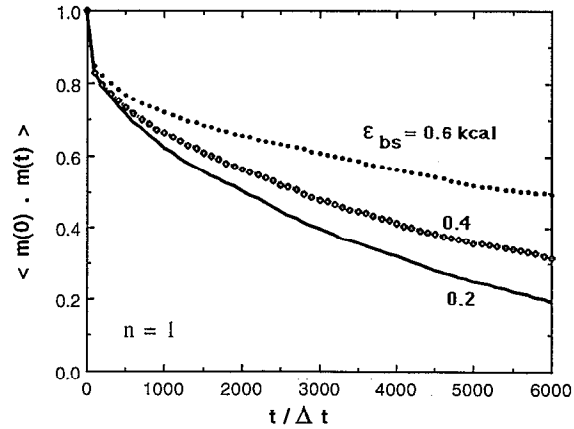

FIG. 9. Influence of solvent–polymer interaction on the orientational relaxation of bond vectors. The time decays of $\langle\mathbf{m}(0)\cdot\mathbf{m}(t)\rangle$ of unit vectors along backbone bonds are shown for $\varepsilon_{bs}/\varepsilon^*=0.2$, 0.4, and 0.6, indicating faster relaxation with decreasing ε_{bs}, i.e., with weaker intermolecular associations.

Figure 10 shows that relaxation rates depend strongly on the size of the chain segment, being faster in the case of more localized motions, i.e., shorter segments, as expected. The slowest relaxation process would occur in the case of $n=N_b-1$. (The latter is not shown in the figure since it decays to about 0.8 only, within the time scale of the figure, and is subject to relatively large fluctuations.) On the other hand, from the comparison of the abscissa in Figs. 4 and 10, we note that the decay of the orientational autocorrelation functions involves time scales which are about 2 orders of magnitude larger than those of the mass center velocity. This feature might appear confusing at first sight, in view of the fact that the mass center diffusion, which is representative of the motion of the chain as a whole, is certainly slower than the orientational relaxation of smaller size chain segments. But although the mass center

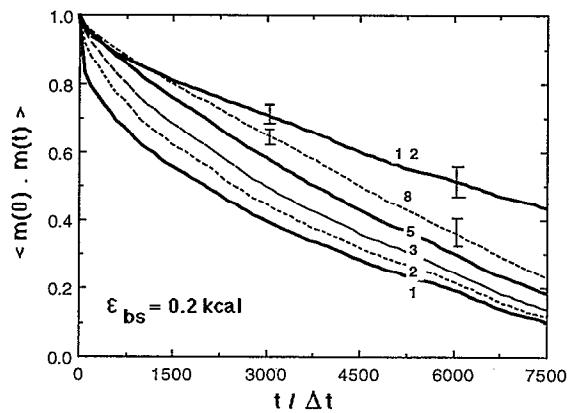

FIG. 10. Time decay of orientational correlation functions $\langle\mathbf{m}(0)\cdot\mathbf{m}(t)\rangle$ for unit vectors along the end-to-end separation of chain segments of n bonds, for $n=1$, 2, 3, 5, 8, and 12, as indicated. Curves are obtained from MD simulations of duration $2.0\times10^5\Delta t$ using the parameters of Table I with $\varepsilon_{bs}=0.2$ kcal/mol. Ensemble averages over the (N_b-n-6) internal segments excluding four units at both ends of the chain are considered in each case. The error bars in the cases of highest noise are shown.

Downloaded 08 Jul 2003 to 136.142.92.33. Redistribution subject to AIP license or copyright, see http://ojps.aip.org/jcpo/jcpcr.jsp

diffusion is in fact slower, this does not imply that the *velocity autocorrelation* curves displayed in Fig. 4 should also be decaying slowly. On the contrary, a faster decay of the velocity autocorrelation functions indicates a slower diffusion process. This is the basis of the Green–Kubo formula, which yields a lower D value when the integration area below the decay curve is smaller, or vice versa. Physically, a relatively fast decay of the velocity autocorrelation function means, in fact, a rapid loss of orientation in space, or a lack of persistence of motion along a given direction, leading to a small overall mean-square displacement, i.e., low diffusivity. Also, we note that the relative time scales of the two Figs. 4 and 10 are in conformity with previous MD simulations using comparable density and temperature conditions.[13]

Simulations of 2×10^5 time steps ($\sim$1 ns) were performed to obtain the decay curves of Fig. 10. Yet, the curves from independent runs exhibit considerable fluctuations, increasing with time and segment size. The statistical error due to finite time averaging in computer experiments has been analyzed by Zwanzig and Ailawadi.[9,47] Accordingly, the MD results for a given normalized correlation function $C(t)$ differ from the exact value $R(t)$ by the equation $R(t)=C(t)\pm(2\tau/T)^{1/2}[1-C(t)]$, where T is the total duration of simulation and τ is the relaxation time associated with the particular correlation function. Thus the statistical error is proportional to $T^{-1/2}$ in general, and increases from 0 at $t=0$ to $(2\tau/T)^{1/2}$ at long times. On the basis of the characteristic times τ of the orientational relaxation of segments of various size, which will be considered in the next paragraph, the highest statistical errors in Fig. 10 are estimated to be $R(t)-C(t)=0.140\pm0.004$ for $n\geqslant8$ at $t=6000\Delta t$, and decreases to 0.081 ± 0.002 at $t=3000\Delta t$. It is pointed out, however, that the error is reduced by a factor of $N^{1/2}$ when an average over N identical, separate particles/functions is possible.[9,47] Although the precision introduced by this approach depends upon the range of correlations in the chain, the extra averaging over several internal chain segments of a given length, as presently performed, reduces further the statistical noise of the correlation functions. For example, the statistical errors at $t=6000\Delta t$ decrease to 0.039 and 0.043 for $n=8$ and 12, respectively, when the extra averaging over (N_b-n-6) internal segments of the chain is performed. These statistical uncertainties are indicated by the error bars in Fig. 10.

The dependence of the rate of orientational relaxation on the size of chain segments involved in local motions has been a subject of interest in previous studies. A correlation time τ may be assigned to each size segment either from the integral of the above time decay curves or from the inverse of their initial slope.[48,49] The second approach is presently undertaken, inasmuch as the correlation function for large n becomes statistically unreliable at long times. The resulting correlation times are plotted in Fig. 11 for $n<8$ and $\varepsilon_{bs}=0.1$, 0.3, 0.5, 0.6, and 0.8 kcal/mol. An almost linear dependence between τ and n is observed in the logarithmic plot of Fig. 11, supporting *the presence of a power law of the form* $\tau\sim n^a$ *between the size and the orientational relaxation time of short chain segments in a given environment.* For $\varepsilon_{bs}=0.1$ kcal/mol, the best fitting line indicates an exponent of $a=1.00$ for the variation $\tau\sim n^a$. The exponent increases with increasing quality of the solvent and equates to 1.46 for $\varepsilon_{bs}=0.8$ kcal/mol.

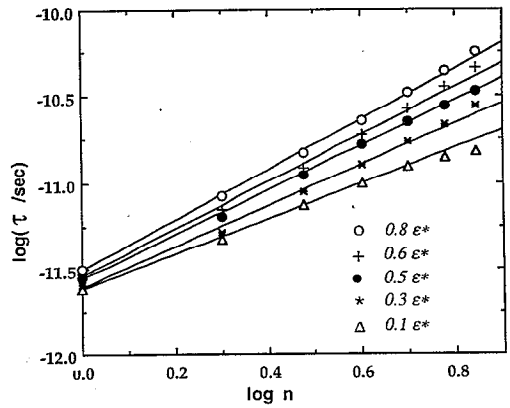

FIG. 11. Dependence of orientational correlation times τ on the size of the chain segment involved in local motion. $\log(\tau/s)$ is plotted against $\log n$ where n is the number of bonds in the segment. A power law of the form $\tau\sim n^a$ is observable, with the exponent decreasing from 1.46 for $\varepsilon_{bs}=0.8\varepsilon^*$ to 1.00 for $\varepsilon_{bs}=0.1\varepsilon^*$, as follows from best fitting straight lines.

In Rouse dynamics, the relaxation times scale as n^2, whereas the Zimm theory yields an exponent of 3ν in the presence of hydrodynamic interactions, ν assuming the values 0.5 and 0.6 in theta and good solvents, respectively. The Rouse–Zimm model is developed for long chains consisting of several Gaussian subchains, and gives a good description of low frequency motions in polymers. In the so-called sub-Rouse regime, on the other hand, which involves small wavelength or intermediate frequency range motions, a weaker dependence on the size of the moving unit is predicted.[50–52] Both analytical[52] and numerical[50] analysis of the dispersion of normal relaxational modes for a segment of $n=16$ coupled bonds indicate that, except for a few slowest modes, a plateau value is approached for the frequency of all relaxational modes, and an almost linear dependence of terminal mode relaxation rate on n is observed up to $n=150$. This weaker dependence of relaxation rate on the size of the kinetic unit, compared to classical Rouse–Zimm model, has been thoroughly discussed in previous work.[52] Arguments on the reduced mobility of short constrained chain segments associated with their smaller number of degrees of freedom, go back to the original work of Kuhn.[30,53] The present simulations lend support to those arguments. The exponent a lies below the Rouse–Zimm values, in general. Furthermore, the present simulations indicate that the exponent, not only assumes lower values in high frequency regime, but also changes depending on the quality of the solvent. Interestingly enough, the lowest exponent is observed here in the case of the most compact chains (i.e., for $\varepsilon_{bs}=0.1$ kcal/mol), which is intrinsically subject to strongest intramolecular constraints. In analogy with the increase of the Zimm exponent from 1.5 to 1.8 with solvent quality, the exponent a shows a systematic

Downloaded 08 Jul 2003 to 136.142.92.33. Redistribution subject to AIP license or copyright, see http://ojps.aip.org/jcpo/jcpcr.jsp

increase as the chain assumes more expanded configurations.

IV. CONCLUDING REMARKS

The present MD study invites to attention the influence of the strength of polymer–solvent interactions on the equilibrium and dynamic properties polymers in dilute solution. Two major effects of solvent quality are observable. First, chain properties are affected on a local scale, i.e., at the level of individual chain units and segments. The changes in pair radial distribution functions illustrated in Figs. 1 and 2, as well as the changes in the bond stretching and orientational mobility displayed in Figs. 3 and 9, respectively, provide firm evidence of the perturbation of chain properties on a local scale. Second, an impact on the chain overall statistics and dynamics is observable. The smooth linear decrease in the translational diffusion coefficient with increasing solvent–polymer attractions, displayed in Fig. 5, is a clear indication of this effect. This figure is considered as a significant result, exhibiting the net effect of solvent quality on chain diffusivity.

The slower relaxation process occurring in media favoring intermolecular interactions is attributed to the overall expansion in chain dimensions, as verified in Fig. 7 by the approximately linear dependence of D on the reciprocal of the radius of gyration, irrespective of ε_{bs}. Inasmuch as the decrease in the relative size of the simulation box might induce a lower mobility due to the enhanced hydrodynamic interactions between the chain and its image, the validity and limitations of our results have been inquired by carrying out repetitive simulations for different R_g/L ratios. Within the range $0.15 \leqslant R_g/L \leqslant 0.25$ investigated, under good solvent conditions, as imparted by the particular set of simulation parameters, the observed change in diffusivity was only marginal, indicating that the observed behavior was justifiable irrespective of the size of the simulation box. Besides, reducing or enlarging the box size would intrinsically induce an increase or decrease in the concentration of the solution, which is incompatible with the hypothesis of a fixed-concentration solution. More specifically, if the increase in R_g arises from a favorable polymer-solvent interaction as in the present case, and not the adoption of a different chain length, this increase should not be suspended by adopting a larger simulation box for the sake of preserving the ratio R_g/L fixed, but on the contrary the resulting enhancement in interchain hydrodynamic interactions should be considered as an indirect effect of the solvent.

The autocorrelation decay functions for internal chain segments of n bonds displayed in Fig. 10 are subject to statistical uncertainties increasing with n and t as indicated by the error bars. However, the results for $n \leqslant 7$ exhibit substantially lower noise, and the corresponding characteristic times presented in Fig. 11 may be considered as statistically reliable estimates of the dependence of relaxation time on segment size. In this respect, it is interesting to find out that a power law of the form $\tau \sim n^a$ applies to local motions, the exponent therein increasing with solvent quality in the range $1.0 < a < 1.5$. An inverse linear relationship between the terminal mode relaxation frequency and the number of bonds cooperatively participating in this localized mode was also pointed out in previous work,[50–52] contrasting the Rouse–Zimm behavior of long Gaussian subchains. Yet, the establishment of these results awaits further experimental and theoretical support.

Approaches considering the structural characteristics of the chain such as the rotational isomeric state model[1] have proven to be valuable for the understanding of chain configurational statistics. To include the influence of solvent as a perturbation has been common practice. Likewise, local chain stochastics has been analyzed with the aid of molecular approaches based on discrete rotameric states accessible to single chain, using the fundamental assumptions and implications of the RIS approach.[54] Although the present approach invites attention to the role and importance of the interaction of polymer chains with the surroundings, it would be desirable to inspect the validity of the same effect in chains subject to real intramolecular conformational potentials. This would lead to an understanding of the relative importance of solvent in systems in which the chain intramolecular constraints are predominantly operative, in contrast to the bead–spring model chains which are devoid of any structural and conformational constraints other than chain connectivity.

[1] P. J. Flory, *Statistical Mechanics of Chain Molecules* (Interscience, New York, 1969).
[2] H. Yamakawa, *Modern Theory of Polymer Solutions* (Harper & Row, New York, 1971).
[3] L. L. Burshtein and T. P. Stepanova, Vysokomol. Soedin., Ser. A **11**, 2885 (1969).
[4] B. Baysal, B. A. Lowry, H. Yu, and W. H. Stockmayer, in *Dielectric Properties of Polymers*, edited by F. E. Karasz (Plenum, New York, 1972).
[5] D. Chandler and L. R. Pratt, J. Chem. Phys. **65**, 2925 (1976); **66**, 147 (1977); L. R. Pratt, C. S. Hsu, and D. Chandler, *ibid.* **68**, 4202 (1978).
[6] A. E. Tonelli and L. A. Belfiore, Macromolecules **16**, 1740 (1983).
[7] I. Bahar, B. M. Baysal, and B. Erman, Macromolecules **19**, 1703 (1986).
[8] J. Pilar and J. Labsky, Macromolecules **24**, 4188 (1991).
[9] M. P. Allen and D. J. Tildesley, *Computer Simulation of Liquids* (Clarendon, Oxford, 1989).
[10] *Computer Simulation of Polymers*, edited by R.-J. Roe (Prentice Hall, New York, 1990).
[11] See, for example, A. Kolinski and J. Skolnick, J. Chem. Phys. **97**, 9412 (1992), and references cited therein.
[12] D. C. Rapaport, J. Chem. Phys. **71**, 3299 (1979); M. Bishop, M. H. Kalos, and H. L. Frisch, *ibid.* **70**, 1299 (1979); **79**, 3500 (1983).
[13] W. Bruns and R. Bansal, J. Chem Phys. **74**, 2064, 5149 (1981).
[14] B. Smit, A. van der Put, C. J. Peters, J. de Swaan Arons, and J. P. J. Michels, J. Chem. Phys. **88**, 3372 (1988).
[15] J. Luque, J. Santamaria, and J. J. Freire, J. Chem. Phys. **91**, 584 (1989).
[16] C. Pierloni and J.-P. Ryckaert Phys. Rev. Lett. **61**, 2992 (1991).
[17] B. Dunweg and K. Kremer, Phys. Rev. Lett. **61**, 2996 (1991).
[18] C. Pierloni and J.-P. Ryckaert J. Chem. Phys. **96**, 8539 (1992).
[19] H. Takeuchi and R.-J. Roe, J. Chem. Phys. **94**, 7446 (1991).
[20] H. Takeuchi and R.-J. Roe, J. Chem. Phys. **94**, 7458 (1991).
[21] D. Rigby and R.-J. Roe, J. Chem. Phys. **78**, 7285 (1987).
[22] H. Takeuchi and K. Okazaki, J. Chem. Phys. **92**, 5643 (1990).
[23] H. Takeuchi, R.-J. Roe, and J. E. Mark, J. Chem Phys. **93**, 9042 (1990).
[24] I. Zuniga, I. Bahar, R. Dodge, and W. L. Mattice, J. Chem. Phys. **95**, 5348 (1991).
[25] R. Dodge and W. L. Mattice, Macromolecules **24**, 2709 (1991).
[26] Y. Zhan and W. L. Mattice, Macromolecules **25**, 1554 (1992).

Downloaded 08 Jul 2003 to 136.142.92.33. Redistribution subject to AIP license or copyright, see http://ojps.aip.org/jcpo/jcpcr.jsp

[27] I. Bahar, N. Neuburger, and W. L. Mattice, Macromolecules **25**, 2992 (1992).
[28] D. Brown and J. H. R. Clarke, Macromolecules **24**, 2075 (1991).
[29] D. Ceperley, M. H. Kalos, and J. L. Lebowitz, Phys. Rev. Lett. **41**, 313 (1978).
[30] P.-G. de Gennes, *Scaling Concepts in Polymer Physics* (Cornell University, Ithaca, 1979).
[31] J.-P. Ryckaert and A. Bellemans, Chem. Phys. Lett. **30**, 123 (1975).
[32] J.-P. Ryckaert, G. Ciccotti, and H. J. C. Berendsen, J. Comput. Phys. **23**, 327 (1977).
[33] T. A. Weber, J. Chem. Phys. **69**, 2347 (1978).
[34] J. Oh, Y. S. Lee, and T. Ree, Bull. Korean Chem. Soc. **4**, 87 (1983).
[35] L. V. Woodcock, Chem. Phys. Lett. **10**, 257 (1970).
[36] T. Schneider and E. Stoll, Phys. Rev. B **13**, 1216 (1976).
[37] D. Evans, J. Mol. Phys. **37**, 1745 (1979).
[38] H. C. Andersen, J. Chem. Phys. **72**, 2384 (1980).
[39] H. J. C. Berendsen, J. P. M. Postma, W. F. van Gunsteren, A. Dinola, and J. R. Haak, J. Chem. Phys. **81**, 3684 (1984).
[40] R. B. Bird, C. F. Curtiss, R. C Armstrong, and O. Hassager, *Dynamics of Polymeric Liquids. Volume 2 Kinetic Theory* (Wiley-Interscience, New York, 1987).
[41] J. H. R. Warner, Ind. Eng. Chem. Fundamentals **11**, 379 (1972).
[42] R. C. Armstrong, J. Chem. Phys. **60**, 724 (1974).
[43] R. W. Hockney and J. W. Eastwood, *Computer Simulation Using Particles* (MacGraw Hill, New York, 1981).
[44] B. H. Zimm, J. Chem. Phys. **24**, 269 (1956).
[45] M. Doi and S. F. Edwards, *The Theory of Polymer Dynamics* (Clarendon, Oxford, 1986).
[46] Cubic simulation boxes of $k=6$, 8, and 10 sites along one edge lead to the respective number of particles $N=N_s+N_b=1.5k^3=324$, 768, and 1500.
[47] R. Zwanzig and N. K. Ailawadi, Phys. Rev. Lett. **182**, 280 (1969).
[48] G. Schwarz, Ber. Bunsenges. Phys. Chem. **75**, 40 (1971).
[49] I. Bahar, B. Erman, and L. Monnerie, Macromolecules **23**, 1174 (1990).
[50] G. Allegra, J. Chem. Phys. **68**, 3600 (1978).
[51] M. Fixman, J. Chem. Phys. **69**, 1527 (1978).
[52] I. Bahar, B. Erman, and L. Monnerie, Macromolecules **24**, 3618 (1991).
[53] W. Kuhn and H. Kuhn, Helv. Chim. Acta **45**, 1533 (1945).
[54] I. Bahar and B. Erman, Macromolecules **20**, 1368 (1987).

Downloaded 08 Jul 2003 to 136.142.92.33. Redistribution subject to AIP license or copyright, see http://ojps.aip.org/jcpo/jcpcr.jsp